Oktarina Heriyani - Perforated concave rectangular winglet pair vortex generators enhance the heat transfer of air flowing through heated tubes inside a channel

by Oktarina Heriyani Uploaded By Lutfan Zulwaqar

Perforated concave rectangular winglet pair vortex generators enhance the heat transfer of air flowing through heated tubes inside a channel

Oktarina Heriyani [a,b,*], Mohammad Djaeni [a], Syaiful [a,**], Aldila Kurnia Putri [a]

[a] Mechanical Engineering Department, Engineering Faculty, University of Diponegoro, Semarang, Indonesia
[b] Mechanical Engineering Program, Engineering Faculty, University of Muhammadiyah Prof. DR. HAMKA, Jakarta, Indonesia

ARTICLE INFO

ABSTRACT

A significant increase in the rate heat transfer in a heat exchanger system is made possible by increasing the convection heat-transfer coefficient using a passive method. The addition of vortex generators (VGs) to the fins and tubes of a heat exchanger is currently the most effective passive method. However, the increase in heat was accompanied by an increase in pressure drop. Therefore, in this study, we installed perforated concave rectangular winglet pair vortex generators (PCRWP VGs) on plates in rectangular ducts to increase the heat transfer through the six heated tubes to the air stream by lowering the enhancement in the pressure drop. We attempted to determine the best cost-benefit ratio (*CBR*) with a fluid flow velocity difference of 0.4–2 m/s at intervals of 0.2 m/s (Reynolds number (*Re*) of 2143 to 11,763) in the channel. The PCRWP VGs were composed of in-line and staggered configurations. The results showed a lower *CBR* (3.56) for the in-line configuration than for the staggered configuration. Moreover, the lowest *CBR* was accompanied by an increase in thermal performance (*TEF*) of 1.29.

1. Introduction

The global energy demand is expected to triple over the next few years. According to a statement by the International Energy Agency (IEA), the main driver is the increasing use of air conditioning (AC) machines [1]. Thus, promoting energy efficiency in air conditioners is important and requires maximising their thermal performance, which involves increasing the rate of heat transfer in its main component, i.e., the condenser. A condenser, commonly used in air conditioners, comprises a fin and a tube and functions as a refrigerant cooling medium. However, the high thermal resistance (75%) of the fin air side of the condenser lowers the heat-transfer rate the heat exchanger [2]. Thus, the thermal resistance must be lowered to enhance the heat transfer rate.

A commonly used active methods to increase the rate of heat transfer involves adding vortex generators (VGs), which, according to the research results obtained by Mugisidi et al., increases the performance of a condenser [3]. The added VGs cause longitudinal vortices (LVs), damage the primary flow, make the second flow as large as the first and increase air mixing in the area [4,5]. The size of the LVs, shape of the flow, and mixing are influenced by the shape, geometry and position of

the VGs added to the fins and tubes of the heat exchanger [6].

Samidifat et al. showed that simple rectangular vortex generators (RVGs) can increase the heat transfer rate by 7%; however, this causes a pressure drop in the heat exchanger system [7]. Meanwhile, modified RVGs with a concave shape on the front and rear surfaces decreased the heat transfer performance of the heat exchanger tube. A better option is to use RVGs with a double convex front surface and a single concave back surface, which can strengthen the primary vortex, increasing the rate of heat transfer from the plate to the fluid, as demonstrated in a study by Kashyap et al. [8]. Further research conducted by Kashyap et al. in the same year concluded that modifying the surface shape of rectangular winglet vortex generators (RWVGs) can create longitudinal eddies that interact with the boundary layer, thereby increasing the rate of convection heat transfer [9]. Based on their research, the increase in the optimal heat transfer rate was 14.4. The optimal heat transfer performance was also obtained from the results of experiments conducted by Adnan et al. on rectangular ducts by adding delta and rectangular winglet VGs [10]. Concave curved delta winglet VGs were compared with convex curved delta winglet VGs by Song et al. to observe changes in the heat transfer rate [11]. The results showed that the concave VGs

---

* Corresponding author. Mechanical Engineering Department, Engineering Faculty, University of Diponegoro, Semarang, Indonesia.
** Corresponding author.
E-mail addresses: oktarina@uhamka.ac.id (O. Heriyani), syaiful.undip2011@gmail.com (Syaiful).

improved the heat transfer better than the convex VGs. The differences in the shape of the VGs affects the change in the heat transfer rate and the change in the geometry of the VG, such as a new rib geometry in the cylinder channel [12].

Zeeshan et al. showed that increasing the angle of attack increased the rate of heat transfer (to 37.01–64.54%) if a pair of RWVGs were placed at the back of the tube even though this did not reduce the pressure drop [13]. A decrease in the value of the pressure drop also did not occur significantly, even though there was an increase in heat of 260% in heat, as per the results of the research conducted by Linardo et al. using the batched heat and channelled pipe (BHCP) approach [14]. The increase in heat transfer performance is influenced by the number of RWVG pairs based on the research results of Heriyani et al., where there is an increase in the hydraulic thermal performance evaluation criteria by 15.17% for three pairs of RWVG compared with the baseline [15]. Wang et al. found that the more pairs of VGs placed in the crossflow, the higher the increase in the heat transfer coefficient [16]. Sun et al. further discovered that increasing the number of RWVGs in the heat exchanger tube increased the heat transfer, with a maximum thermal enhancement factor (TEF) of 1.27 [17]. The TEF value of a V-delta winglet VG reached 1.82–3% higher than that of a V-rectangular winglet VG, as revealed by Promvonge et al. [18]. These results were obtained with an optimal blockage ratio (BR) of 0.15 and pitch ratio (PR) 1.0. Skullong et al. modified the shapes of RWVGs with optimal BRs and PRs to achieve an optimum heat transfer performance and reduced pressure drop; their shape modification involved perforating RWVGs [19].

The positions of the holes in the RWVGs did not significantly affect the increase in heat transfer; however, they significantly affected the flow resistance of the VGs. The heat-transfer rate increased as the height (vertical position) of the hole increased. Widthwise, although there is an initial increase, the heat transfer rate decreased with increasing lateral distance [20]. An increase in the number of holes in the RWVGs indicates an increase in fluid flow, which forces the fluid to flow behind the RWVGs, thereby increasing heat transfer [4]. The heat transfer rate increased during laminar flow when the Reynolds number (Re) increased and then decreased with an increase in Re during turbulent flow [23]. Positioning the tube in-line with a pair of RWVGs in a common flow-down configuration provides better performance than the common flow-up configuration. However, a staggered tube position is

superior, resulting in a 25.85% higher heat-transfer performance than when a pair of RWVGs is not used [21].

In the existing studies, no detailed analyses of heat transfer were conducted on from the surfaces of several cylinders heated and arranged in-line with using a perforated vortex generator. Therefore, the focus herein is on investigating the advantages of using perforated concave rectangular winglet pair vortex generators (PCRWP VGs) to increase the heat transfer of the airflow through heated tubes arranged in-line in the ducts.

2. Experimental approach

2.1. Experimental setup

This research was conducted experimentally with a test equipment scheme comprising a rectangular channel sized 370 × 18 × 8 cm. The duct was made of 1 cm thick glass, as shown in Fig. 1.

Based on Fig. 1, the rectangular channel is equipped with a blower (50 Hz, Wipro with a rated voltage of 220 V), an inverter (Mitsubishi Electric type FR-D700 with an accuracy of 0.01), straightened, hot wire anemometer (Lutron type AM-4204 with an accuracy of 0.1), wattmeter (Lutron DW-6060 with an accuracy ± 1.0), central processing unit (CPU), micromanometer, thermocouple (K type with a temperature interval of $-200 - 1250\,°C$ and an accuracy ± 0.5) where one thermocouple was placed in the air inlet area, six thermocouples on the back surface of the tubes and 15 on the outlet side of the wire, data acquisition (Advantech USB-4718 type with an accuracy of 0.001) and heater regulator. The heater was connected to six tubes with a diameter of 19.05 mm and height of 65.8 mm, with each tube having the same power. Total heating power of 40 W was applied to the six tubes using a regulator. The heating air flowing through the tubes occurs via convection. Thus, the air at the outlet side becomes hotter than that at the inlet side.

A pressure micromanometer (Fluke type 922, with an accuracy of ±0.05) was used to monitor the flow pressure drop. Two pitot tubes, each set 26 cm ahead of the inlet of the test specimen and 2.5 cm behind it, were connected to a micromanometer to measure the pressure drop. The pressure drop measurements were recorded 30 times for 5 sekon at each speed variation. Furthermore, flow visualisation was performed by
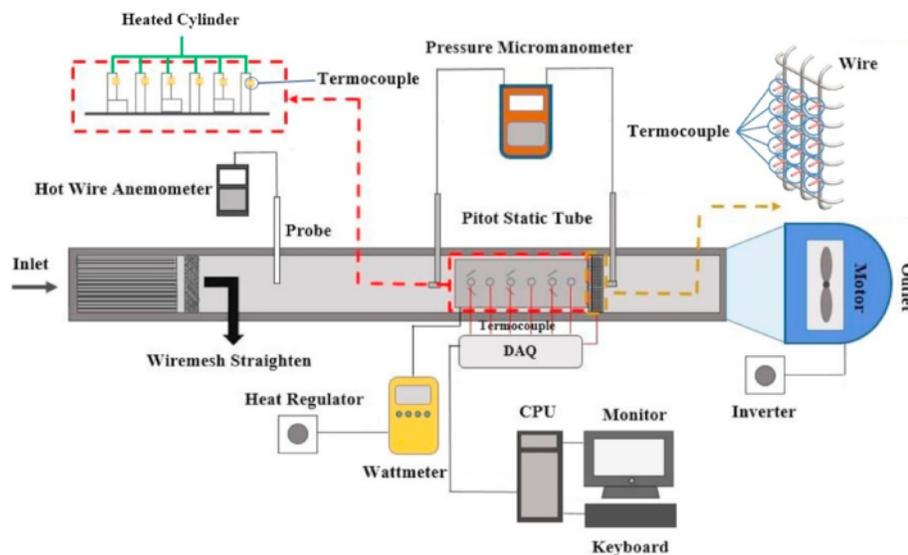

Fig. 1. Experimental tool schematic.

directing the smoke from vaporised fluid in the fluid vaporator into the mainflow.

The VGs used as test specimens were perforated rectangular winglet pair (PRWP) and perforated concave rectangular winglet pair (PCRWP) vortex generators (VGs). Perforated is a term for holes in the VGs, as shown in Fig. 2. The VGs have dimensions of the same length and width of 30 mm, with 36 holes. The bore diameter on the VGs was 2.5 mm. The distance between the holes was 5 mm from the center.

The VGs are placed on an aluminium plate measuring 500 × 165 × 1 mm. The geometry and the pitch between VGs for both in-line and staggered configurations are shown in Fig. 3, with an angle of attack (α) of 150 [2]. The distance between the cylinders is 120 mm, with a cylinder diameter of 19.05 mm.

The VGs configurations were arranged in-line and staggered on the plate. The perforated rectangular winglet (PRW) and perforated concave rectangular winglet (PCRW) VGs in-line configurations with one, two and three pairs are shown in Fig. 4. For each pair, the VGs were placed on the left and right sides of the first row of tubes. VGs were placed in the first- and third-row tubes for two pairs. For the three pairs, VGs were placed on the first-, third-, and fifth-row tubes.

The PRW and PCRW VGs staggered configurations with one, two, and three pairs are shown in Fig. 5. For one pair, the VGs are placed on the right side of the first-row tube and on the left side of the second. The VGs are placed on the right side of the first and third row tubes and on the left side of the second and fourth tubes for two pairs. For the three pairs, the VGs are placed on the right side of the first, third and fifth rows of the tubes and on the left side of the second, fourth and sixth tubes.

2.2. Parameter definitions

The parameters in this study were derived from the equation used by Oneissi et al. to obtain the thermal enhancement factor (TEF) [22].
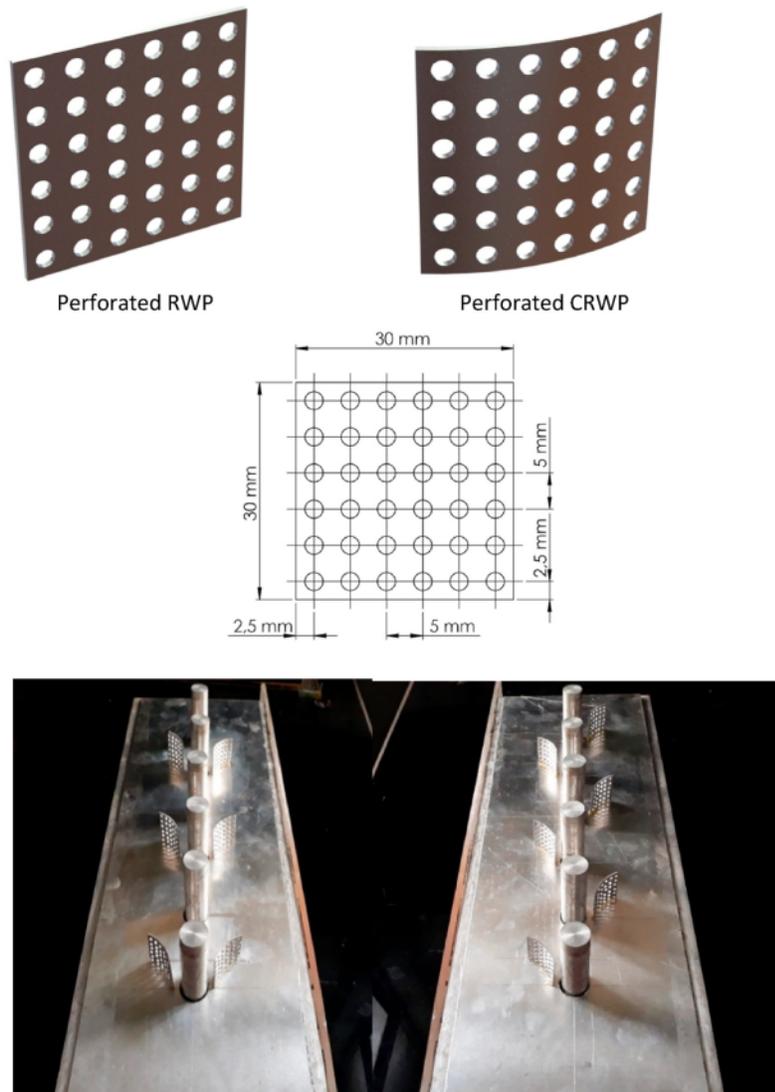
Perforated RWP   Perforated CRWP

Fig. 2. Geometry of the VGs.

Fig. 3. Geometry and pitch of the VGs.

$$TEF = \frac{\frac{Nu}{Nu_0}}{\left(\frac{f}{f_0}\right)^{\frac{1}{3}}} \tag{1}$$

The Nusselt number dan friction factor for the baseline conditions are symbolised as (Nu_o) and (f_0), and (Nu) and (f) based on the research of Zeeshan et al. [23]

$$Nu = \frac{q \, D_h}{A_{tube} \, \Delta T_{LMTD} \, k} \tag{2}$$

$$h = \frac{q}{A_{tube} \, \Delta T_{LMTD}} \tag{3}$$

$$q = \dot{m} \, c_p \, (T_{out} - T_{in}) \tag{4}$$

where D_h, A_{tube}, ΔT_{LMTD}, $\dot{m}$, c_p, T_{out} and T_{in}, are hydraulic diameter, tube surface area, log mean temperature difference, mass flow rate, specific heat, outlet temperature, and inlet temperature, respectively

$$D_h = \frac{4A_c}{p} = \frac{4ab}{2(a+b)} = \frac{2ab}{a+b} \tag{5}$$

$$\Delta T_{LMTD} = \frac{(\overline{T}_{tube} - \overline{T}_{out}) - (\overline{T}_{tube} - \overline{T}_{in})}{\ln[(\overline{T}_{tube} - \overline{T}_{out}) - (\overline{T}_{tube} - \overline{T}_{in})]} \tag{6}$$

where A_c dan T_{tube} are channel surface area and tube temperature, respectively.

The result of D_h is used to calculate Re with the formula

$$Re = \frac{\rho u_{in} D_h}{u} \tag{7}$$

and friction factor (f) was determined to evalute the performance of hydro dynamic using

$$f = \frac{2\Delta P \, D_h}{\rho \, V^2(L + 6D)} \tag{8}$$

where ρ, V, and L are the air density, inlet airflow velocity and length of the test specimen, respectively.

The equation required to determine the cost-benefit ratio (CBR), defined as the ratio of pressure drop per variation in Nu number, as formulated by Tian et al. [25], is as follows:

$$CBR = \frac{\%\Delta P}{\%Nu} \tag{9}$$

This concept investigates whether the method used to enhance the heat transfer rate is economically efficient. In the hydrodynamic test, the pressure drop (ΔP) is measured by the pressure difference on the sides of P_{inlet} and P_{outlet} of the test specimen in the tested part using equation (10):

$$\Delta P = P_{inlet} - P_{outlet} \tag{10}$$

2.3. Validation

The current study is a follow-up investigation to the work of Yafid et al. [24], and the experimental setup was similar to that of Yafid et al. The difference between the current study and the experiment of Yafid et al. is a test object in which the current study uses concave rectangular winglet (CRW) VGs; in Yafid et al's experiment concave delta winglet (CDW) VGs are used. Whitaker et al. [25] studied the heat transfer characteristics of airflow through a single cylinder in a rectangular duct. The results of Yafid et al. were valid, and the same experimental set-up was determined. The Nu value from the experiment of Yafid et al. were comparable with the Nu values from the experiments of Whitaker et al. in the Reynolds number (Re) range of 2143 to 11,763.
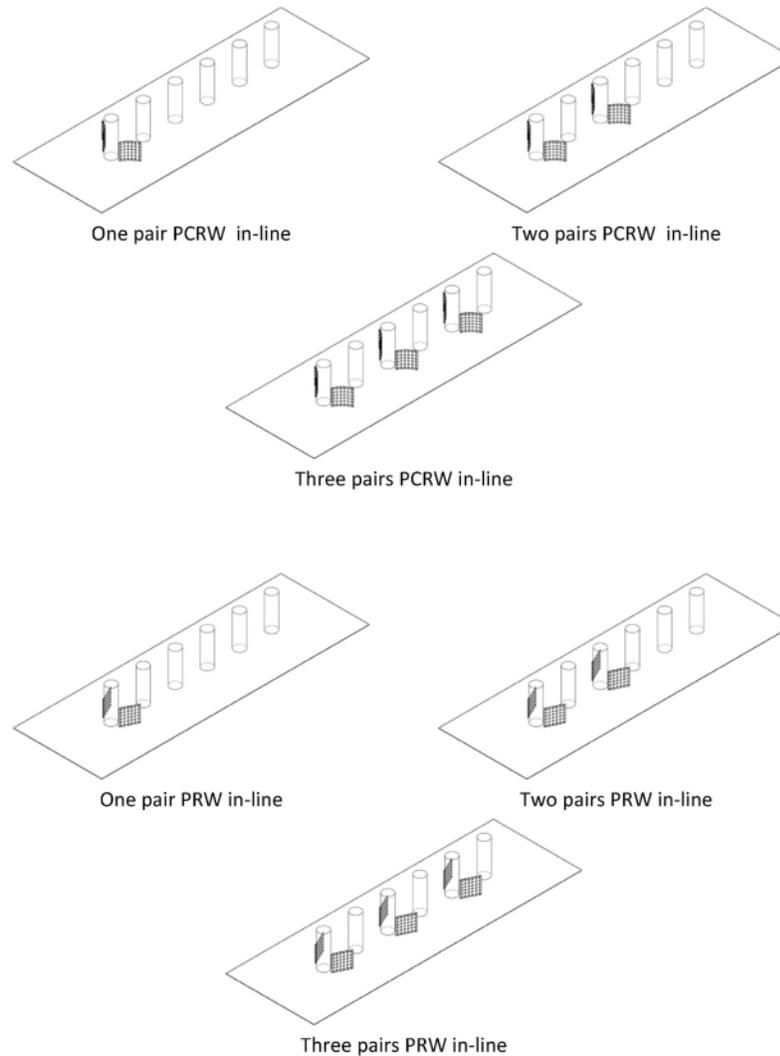
Fig. 4. VGs pairs in-line configurations.

3. Results and discussion

3.1. Flow visualisation

A flow visualisation test was performed to observe the longitudinal vortices (LV) formed after the flow passed through the VGs in the rectangular channel. This test was conducted under low-light conditions to clarify the LV. The laser beam was refracted by a cylindrical glass (diameter 5 mm), which produced a cross-sectional area perpendicular to the direction of the flow. Smoke formed from the evaporation of the liquid was used to visualise the LV in the flow. The VGs used in this visualisation test were PRWP and PCRWP with an in-line arrangement, as shown in Fig. 6.

In Fig. 6 (c) and (d), the PCRWP VGs appear to produce longitudinal vortices (LV) in a wide flow area compared with the PRWP VGs in Fig. 6 (a) and (b) downstream. The back region of the PCRWP VGs had a wider frontal surface area than the PRWP VGs. Consequently, mixing the near-fluid the channel walls with the fluid in the mainstream is better, meaning that the heat transfer rate is increased [26]. Downstream, the

LV compression in the wake area increases the fluid flow velocity passing through the cylindrical structure, thereby increasing the heat transfer rate from the channel surface to the fluid flow in the wake region [27]. The increase in heat transfer produced when using PCRWP VGs was better than that with PRWP VGs.

3.2. Perforated vortex generators effect on heat transfer

The increase in the convection heat transfer was due to the mixing of fluids caused by the strong longitudinal vortices (LVs) [28]. The strength of the LVs is caused by the amount of VGs sets; increasing the amount of VGs pairs in the test specimen can increase the coefficient of the convection heat transfer [29], as shown in Fig. 27.

In Fig. 7, we can see the convective heat transfer coefficient with respect to the Reynolds number (*Re*), analysed after installing the PCRWP and PRWP with pairs ranging from one, two and three, arranged in-line or staggered. Based on Fig. 7, the convective heat transfer coefficient increased with a rise in *Re* due to an increase in flow vortices and high turbulence intensity in the channel [30], alongside a reduction in
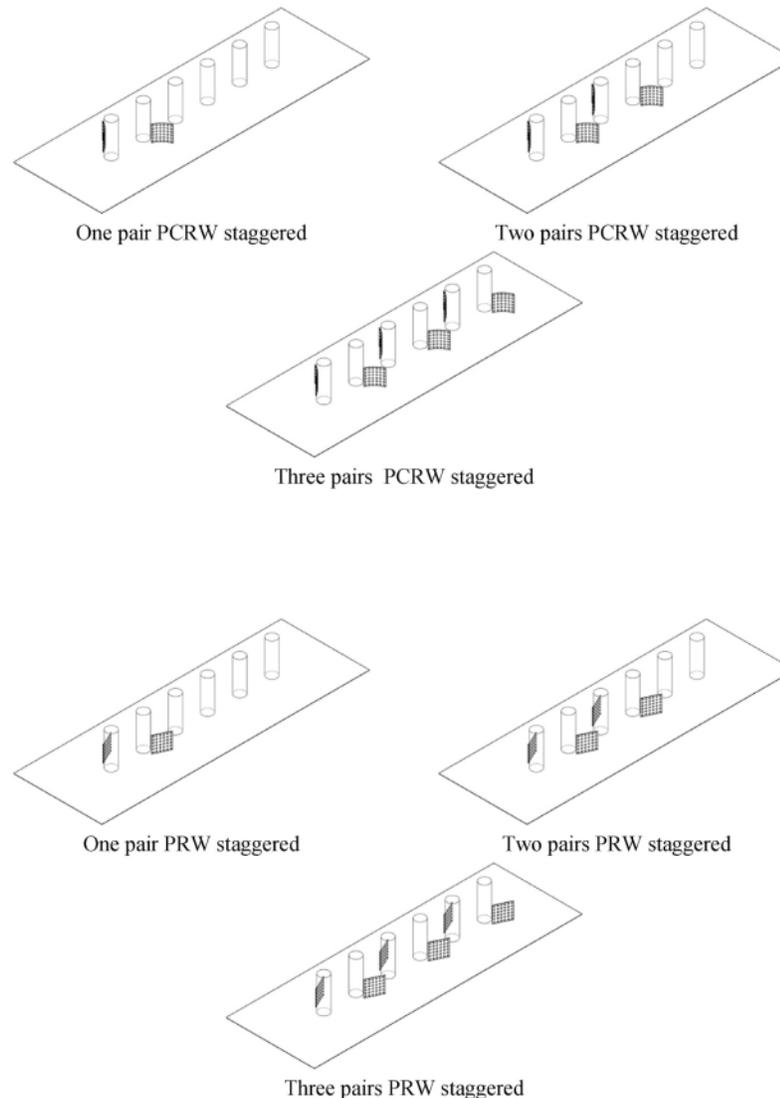
Fig. 5. VGs pairs staggered configurations.

the wage region and stagnation area for each increase in flow velocity [31]. The improve in heat transfer for the staggered was better than that for the PCRW VGs with any number of pairs at the highest *Re* (11,000). The results in Fig. 7 show that the PCRWP VGs worked better than the PRWP VGs, and the staggered arrangement of the former, with three pairs, gave the highest yield (153.5 W/m² • K), as shown in Fig. 7(c). Two PCRW pairs (137.33 W/m² • K, Fig. 7(b)) were better than one (132.25 W/m² • K) (Fig. 7(a)) because the VGs with a concave surface destabilise the force of centrifugal of the fluid flow, strengthening the flow vortices and making the mixing of the hot fluid near the wall with the cold fluid of the main flow more robust [32]. In Fig. 7(a), the convection heat-transfer coefficient for the case of the in-line PRW VGs has the same value as that of the in-line or staggered PCRW VGs in a pair of VGs. In one pair of VGs, a longitudinal vortex is generated after the flow hits and weakens the VGs [29]. This result contrasts with the cases with two and three pairs of VGs, where the longitudinal vortex produced after striking the first VGs is amplified again when the flow strikes the second

VGs and so on. Therefore, the value of the heat transfer coefficient in the case of a pair of PRW VGs is the same value as that of PCRW VGs at Reynolds numbers above 8000.

3.3. Effect of perforated vortex generators on pressure drop

Using VGs can affect the increase in heat transfer, but there is often an accompanying increase in pressure drop, as shown in Fig. 8, where an increase in pressure drop can be seen along with the increases in *Re* and pair numbers for both the VG types PCRW and PRW. In general, the highest pressure drop was observed using the PCRWP VGs with a staggered configuration for all *Re*, except for one pair of VGs. The highest pressure drop was found in the PRWP VGs with an in-line configuration at *Re* greater than 8000. The pressure drop on the staggered VGs was found to be higher than that on the in-line configuration because of the shorter distance between the VGs of the staggered configuration than that of the in-line [29], caused by the resistance of fluid flow against the
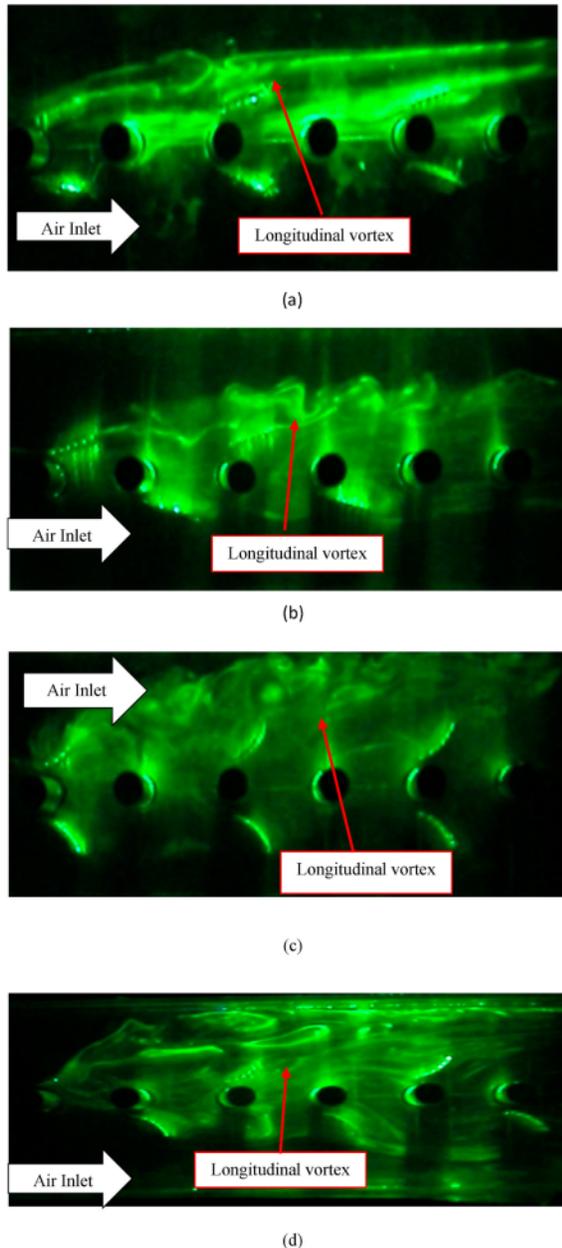
Fig. 6. Visualisation of LV generated by (a) in-line PRWP, (b) staggered PRWP, (c) in-line PCRWP and (d) staggered PCRWP.

walls of the VGs and the expansion of the frontal zone of the VGs in the next-pair arrangement [33]. The pressure drop in the staggered arrangement was lower than that in the in-line arrangement, whereas the PRW VGs type created a lower pressure drop than the PCRW VGs because the latter reduced the frontal area hit by the airflow, resulting in a decrease in drag [34]. In addition, the jet flow from the VG hole can reduce the stagnation flow, which can reduce the pressure drop [35]. A significant decrease in the pressure drop was due to the VG perforation [36]. The best pressure drop value for one pair with a staggered arrangement was 4.58 Pa (see Fig. 4(a)), whereas two pairs (5 Pa, Fig. 4

(b)) were better than three (5.4 Pa, Fig. 4(c)).

3.4. Effect of perforated VGs on thermal enhancement factor

TEF exhibited the hydraulic thermal performance while using VGs, which played a role in restructuring the incoming fluid flow pattern. The increase in the *TEF* was due to the influence of complex overlapping structures, which meant that the flow developed into a turbulent structure, significantly affecting the heat transfer increase [37]. The experimental *TEF* values are shown in Fig. 9.

The *TEF* is the thermal-hydraulic performance which is the ratio of the increase in heat transfer to the pressure drop ratio. In general, the highest *TEF* was observed when the PCRWP VGs were used with a staggered configuration, as depicted in Fig. 9. The PCRW creates wider flow vortices that can reduce the wake area behind the cylinder. Reducing the wake area can reduce the recirculation zone, affecting the heat transfer from the back of the cylinder to the stream [26]. A large-radius, high-intensity anterior-posterior vortex can reduce the wake area. A lessening within the wake zone increased the flow velocity behind the tube and reduced the recirculation area, resulting in increased heat transfer in this area [27,38]. As shown in Fig. 9, there was an increase in the *TEF* with greater pairs of VGs used for both the PCRW and PRW VG because the PCRW produced wider flow vortices, which reduced the wake region behind the cylinder, thereby reducing the recirculation zone and impacting the heat transfer increment from the rear cylinder surface to the stream [39]. In this process, a large number of longitudinal vortices with high intensities can reduce the wake area, which increases the flow velocity downstream of the tube and reduces the recirculation region, leading to an increased heat-transfer rate in the region [40,41]. Based on Fig. 9, the best *TEF* increase occurred at Re between 8000 and 9000. The best *TEF* values, with one, two and three pairs occurred in the staggered arrangement with PCRW VGs, at 1.18, 1.20 and 1.29, respectively (see Fig. 9).

3.5. Effects of perforated VGs on the cost-benefit ratio

Economic evaluation cannot be conducted based only on the *TEF* and the net profit from the heat load of the transferred unit [26]. Instead, it must be determined by evaluating the economic value of the heat-transfer improvement by calculating the cost benefit ratio (*CBR*), as shown in Fig. 10.

Fig. 10 show the result of the *CBR* calculation to compare the percentage increase in the pressure drop with the percentage increase in the Nusselt number when using VGs. These results indicate that a lower *CBR* improves thermal performance, which is greater than the drag force [25]. The greatest increase in *CBR* occurred with the PRW VGs, with an in-line arrangement, totalling 4.57, 4.95 and 3.56 for one, two and three pairs, respectively. The lowest *CBR* was measured when three sets of PCRW vortex generators with a staggered arrangement were used. The lowest *CBR* were obtained with the three pairs of staggered-type VGs PCRW. The three VG pairs showed a lower *CBR* than the one and two pairs because they resulted in the greatest increase in the Nusselt number, accompanied by a lower pressure drop increase, which lowered the *CBR*. These results show that a lower *CBR* improves thermal performance relative to resistivity [26]. A low value *CBR* indicates a more economical value using VGs. In general, using PCRWP VGs with a staggered configuration is the best.

3.6. Heat loss analysis

Heat loss analysis was performed by considering the convection heat transfer from the six tubes to the surrounding fluid flow. The heat transfer rate was calculated for laminar and turbulent flows.

The heat loss in this experiment was calculated by calculating the difference between the induced electric power and total heat through convection from the surface of the tubes to the fluid. In this experiment,
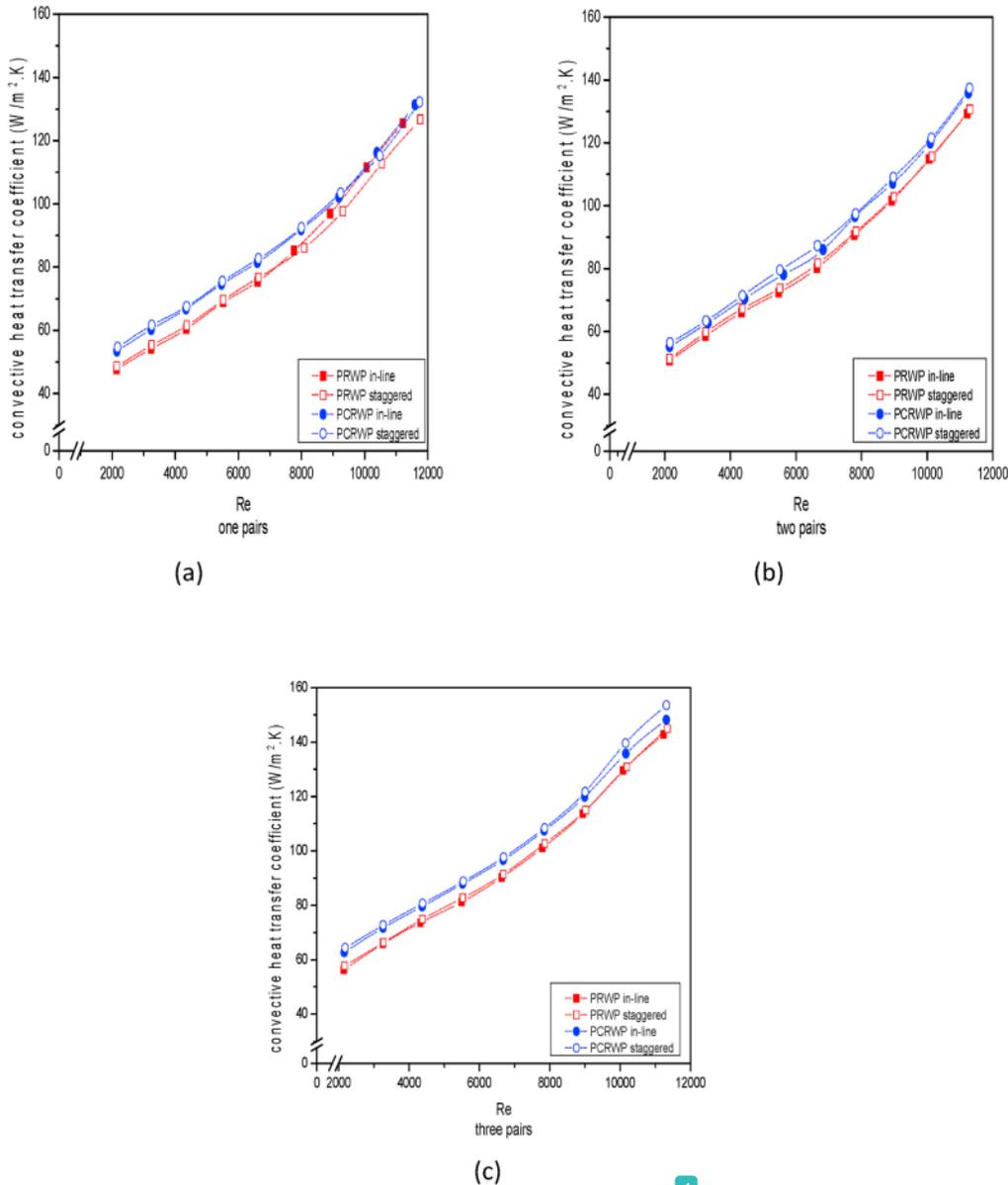
Fig. 7. Graphs of convective heat-transfer coefficient against Reynolds number: (a) one, (b) two and (c) three pairs.

six tubes in a wind tunnel were heated using a heater at a power of 40 W; the velocity of the inlet fluid is varied from 0.4 to 2 m/s at intervals of 0.2 m/s or in the Reynolds number range from 2143 to 11,763. Based on the Reynolds number range, two types of flows were determined; laminar and turbulent. Therefore, the heat loss was determined from the correlation between laminar at 0.4 m/s and turbulent for other velocities. The experimental data for the hydraulic diameter D_h, tube surface area A_{tube}, channel surface area A_c and air specific heat c_p are 0.09223 m, 0.02338908 m^2, 0.01056 m^2 and 1.007 J/kgK, respectively. Table 1 is a baseline for calculating heat loss

From Table 1, the greater the velocity with an increase in the Re, the lower the heat loss. It can be observed that the heat flow from the heater not only spreads into the tube, but convection also occurs outside the

tube. The heat output increased with Re, i.e, the higher the flow velocity, the greater the turbulence through the cylinder and the higher the turbulence intensity. An increase in the turbulence intensity between a cold airflow and hot cylinder with a constant surface temperature is caused by the airflow velocity [26]. In row-tube arrays, this recirculation area increased for the second and subsequent columns. A lower air velocity in the circulation region indicated less airflow in the region participating in the local heating process [37]. The heat loss under all conditions in this experiment is listed in Table 2.
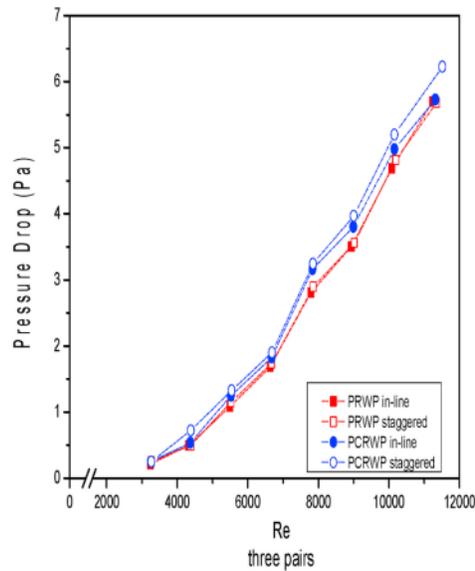
Table 2 shows that the lowest heat loss occurs when three sets of PCRWPs are staggered. The placement of the VGs can increase heat transfer in square ducts as the VGs create longitudinal vortices, which in turn increase vortex strength in the wake region downstream of the tube.

8
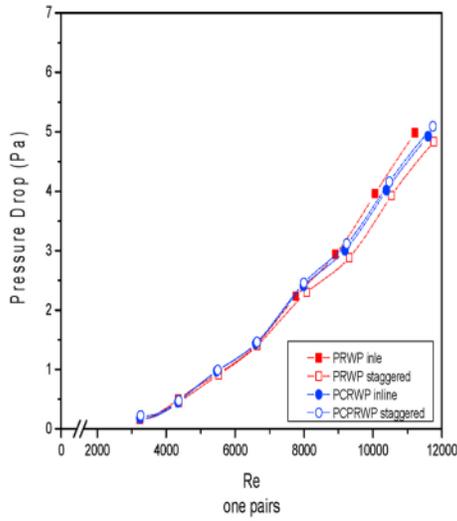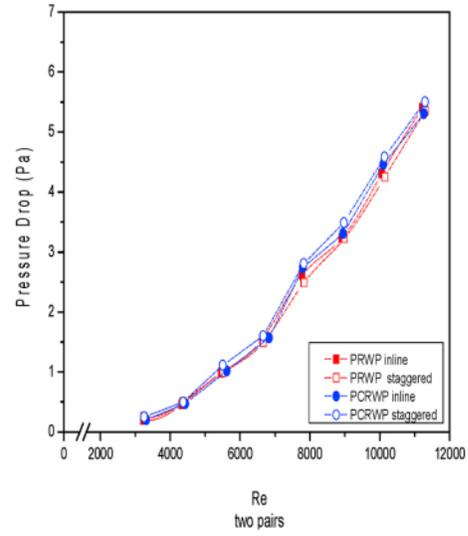
Fig. 8. Graph of pressure drop against Reynolds number: (a) one, (b) two and (c) three pairs.

Longitudinal vortices make the overall temperature field more uniform, improve heat mixing and boundary layer modification, and improve heat transfer performance. A higher number of vortex generators creates more longitudinal vortices and significantly increases heat transfer [26, 29].

3.7. Uncertainty analysis

In this section, uncertainty analysis calculation data will be shown for the temperature at base-line conditions with a velocity of 0.4 m/s as shown in Table 3.

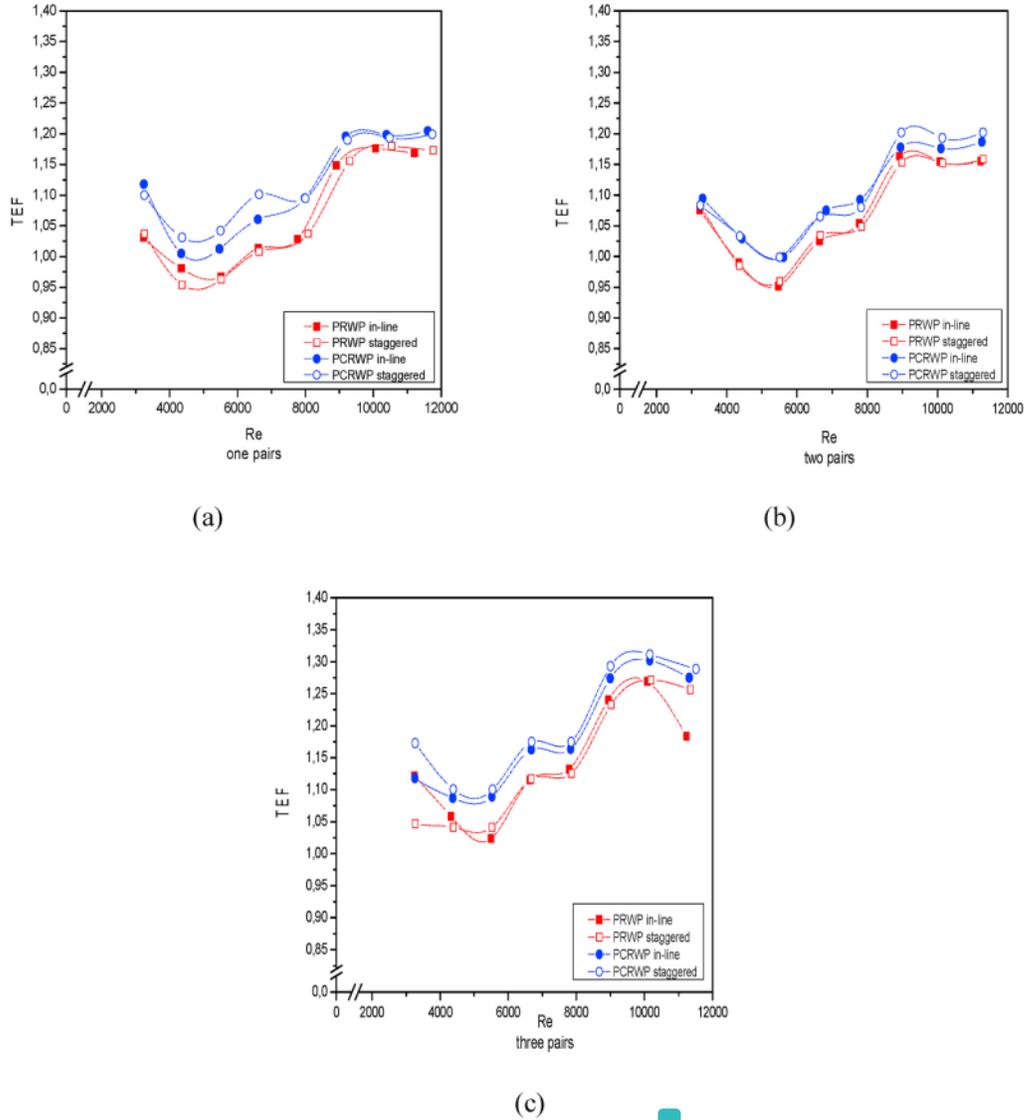From these data, it is found that $\overline{T}_{Tube}$ can be calculated by the equation as

(a)

(b)

(c)

Fig. 9. Graph of thermal enhancement factor against Reynolds number: (a) one, (b) two and (c) three pairs.

$$\overline{T}_{Tube} = \frac{\overline{T}_{Tube1} + \overline{T}_{Tube2} + \overline{T}_{Tube3} + \overline{T}_{Tube4} + \overline{T}_{Tube5} + \overline{T}_{Tube6}}{6} = 49.56°C \quad (11)$$

Then, the average standard deviation is obtained by the following formula.

$$s_{tube} = \sqrt{\frac{\sum_{i=1}^{N}(T_{tubei} - \overline{T}_{tube})^2}{N(N-1)}} = 0.029 \quad (12)$$

Therefore, the average T_{tube} can be written as 49.5 ± 0.029 °C. $\overline{T}_{out}$ calculation results obtained 32.95 °C. The average standard deviation was calculated using the following equation:

$$s_{Tout} = \sqrt{\frac{\sum_{i=1}^{N}(T_{outi} - \overline{T}_{out})^2}{N(N-1)}} = 0,051 \quad (13)$$

Furthermore, the average value of T_{out} can be written as $32.95 \pm$

0.051 °C. Using the same equation, the standard deviation of T_{in} was found to be 0.033. Thus, the average T_{in} value was 29.75 ± 0.016 °C. The value of q at a speed of 0.4 m/s was found to be 19.48 W. To determine of the standard deviation of q, the following equation was used:

$$RSS_q = \sqrt{\left(s(\Delta T_{out})\frac{\partial q}{\partial T_{out}}\right)^2 + \left(s(\Delta T_{in})\frac{\partial q}{\partial T_{in}}\right)^2} \quad (14)$$

$$\frac{\partial q}{\partial T_{out}} = \frac{\partial(m \bullet c_p \bullet T_{out} - m \bullet c_p \bullet T_{in})}{\partial T_{out}} = m \bullet c \bullet p$$

$$\frac{\partial q}{\partial T_{in}} = \frac{\partial(m \bullet c_p \bullet T_{out} - m \bullet c_p \bullet T_{in})}{\partial T_{in}} = -(m \bullet c \bullet p)$$

where $s(\Delta T_{out}) = 0.051°C$ and $s(\Delta T_{in}) = 0.033°C$, ensuring, that $RSS_q =$
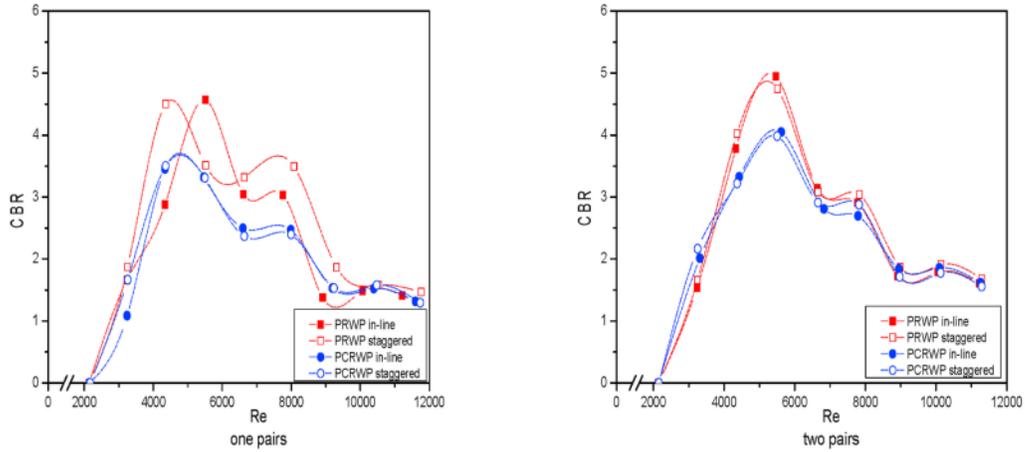
(a)

(b)
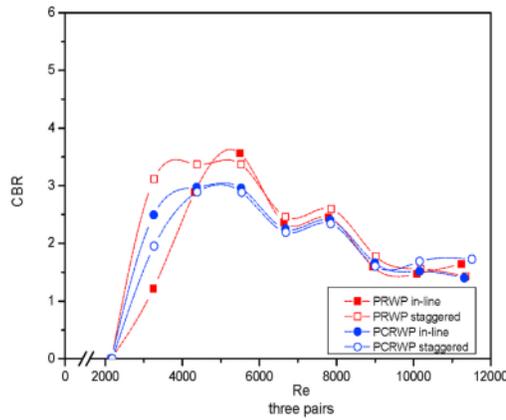
(c)

Fig. 10. Graph of cost-benefit ratio against Reynolds number: (a) one, (b) two and (c) three pairs.

$\pm\,0.290$ W. Therefore, the heat transfer rate q becomes 19.48 ± 0.290 W. The value of ΔT_{lmtd} at a speed of 0.4 m/s was found to be 18.56 °C. To determine the value of the standard deviation of ΔT_{lmtd} we used the following equation:

$$\frac{\partial(\Delta T_{lmtd})}{\partial T_{out}} = \frac{\partial\left(\frac{(T_{tube}-T_{out})-(T_{tube}-T_{in})}{\ln\frac{T_{tube}-T_{out}}{T_{tube}-T_{in}}}\right)}{\partial T_{out}}$$

$$RSS_{\Delta T_{lmtd}} = \sqrt{\left(s(\Delta T_{tube})\frac{\partial(\Delta T_{lmtd})}{\partial T_{tube}}\right)^2 + \left(s(\Delta T_{out})\frac{\partial(\Delta T_{lmtd})}{\partial T_{out}}\right)^2 + \left(s(\Delta T_{in})\frac{\partial(\Delta T_{lmtd})}{\partial T_{in}}\right)^2} \tag{15}$$

$$\frac{\partial(\Delta T_{lmtd})}{\partial T_{tube}} = \frac{\partial\left(\frac{(T_{tube}-T_{out})-(T_{tube}-T_{in})}{\ln\frac{T_{tube}-T_{out}}{T_{tube}-T_{in}}}\right)}{\partial T_{tube}}$$

$$\frac{\partial(\Delta T_{lmtd})}{\partial T_{in}} = \frac{\partial\left(\frac{(T_{tube}-T_{out})-(T_{tube}-T_{in})}{\ln\frac{T_{tube}-T_{out}}{T_{tube}-T_{in}}}\right)}{\partial T_{in}}$$

Table 1
Heat loss baseline.

	v (m/s)	Re	Mass flow rate (kg/s)	Density (kg/m³)	Dynamics viscous (kg/ms)	Pr	k	T inlet (C)	T outlet (C)	T tube (C)	ΔT LMTD	ΔT (T tube - T inlet)	Nu	h (W/mK)	q conv (W)	q input (W)	q loss (W)
baseline	0.4	2165	0.004757	1.13	1.9.E−05	0.73	0.03	29	33	50	19	21	155	45	19.48	40	20.52
	0.6	3291	0.00719	1.13	1.9.E−05	0.73	0.03	28	31	46	16	18	174	50	18.98	40	21.02
	0.8	4413	0.009618	1.14	1.9.E−05	0.73	0.03	28	30	44	15	16	192	50	19.19	40	20.81
	1	5545	0.012056	1.14	1.9.E−05	0.73	0.03	28	30	43	14	15	214	55	19.84	40	20.16
	1.2	6661	0.014477	1.15	1.9.E−05	0.73	0.03	28	29	43	14	15	228	61	21.15	40	18.85
	1.4	7826	0.016958	1.15	1.9.E−05	0.73	0.03	27	29	41	12	13	247	70	20.30	40	19.70
	1.6	8965	0.019407	1.15	1.9.E−05	0.73	0.03	27	28	40	12	13	263	75	21.03	40	18.97
	1.8	10,110	0.021863	1.15	1.9.E−05	0.73	0.03	27	28	39	12	12	296	84	22.54	40	17.46
	2	11,272	0.024341	1.15	1.9.E−05	0.73	0.03	27	28	38	11	11	342	97	24.17	40	15.83

Table 2
Calculation of heat loss for the whole case.

type VGs	q conv (W)	q input (W)	q loss (W)
Baseline	20.74	40	19.26
PCRWPI1	25.15	40	14.85
PCRWPI2	27.55	40	12.45
PCRWPI3	27.61	40	12.39
PCRWPS1	26.43	40	13.57
PCRWPS2	26.43	40	13.57
PCRWPS3	27.94	40	12.06
PRWPI1	24.09	40	15.91
PRWPI2	27.25	40	12.75
PRWPI3	28.82	40	11.18
PRWPS1	23.94	40	16.06
PRWPS2	26.37	40	13.63
PRWPS3	28.12	40	11.88

Table 3
Base-line test temperature data at a speed of 0.4 m/s.

T (Tube$_1$)	T (Tube$_2$)	T (Tube$_3$)	T (Tube$_4$)	T (Tube$_5$)	T (Tube$_6$)
49.19093	51.21368	48.32313	49.76915	47.80219	51.27142
49.1834	51.17728	48.3156	49.79053	47.7657	51.2639
49.14545	51.16826	48.30655	49.7526	47.7856	51.25489
49.12105	51.17277	48.28214	49.72821	47.76118	51.2594
49.15297	51.20465	48.28515	49.73122	47.73524	51.2624
49.09966	51.15141	48.28967	49.73573	47.76871	51.26691
49.09815	51.14991	48.23029	49.73423	47.73826	51.29428
49.08912	51.14089	48.25019	49.66739	47.72922	51.22751

where $s(\Delta T_{tube}) = 0,029°C$, $s(\Delta T_{out}) = 0,051°C$ and $s(\Delta T_{in}) = 0,033°C$; we get $RSS_{\Delta T_{lmtd}}$ of ±0.043, ensuring, that the obtained ΔT_{lmtd} is 8.56 ± 0.043.

The value of Nu at a speed of 0.4 m/s was found to be 155.31. The standard deviation of Nu was obtained using following equation

$$RSS_{Nu} = \sqrt{\left(s(q)\frac{\partial Nu}{\partial Q}\right)^2 + s(\Delta T_{lmtd})\frac{\partial Nu}{\partial \Delta T_{lmtd}}} \quad (16)$$

$$\frac{\partial Nu}{\partial q} = \frac{\partial\left(q \bullet D_h.At^{-1} \bullet \Delta T_{lmtd}^{-1} \bullet k^{-1}\right)}{\partial q} = \frac{D_h}{(At)(\Delta T_{lmtd})(k)}$$

$$\frac{\partial Nu}{\partial \Delta T_{lmtd}} = \frac{\partial\left(q \bullet D_h \bullet At^{-1} \bullet \Delta T_{lmtd}^{-1}.k^{-1}\right)}{\partial \Delta T_{lmtd}} = \frac{q.D_h}{(At)(\Delta T_{lmtd})^2(k)}$$

With the values of $s(q) = 0.290\ W$ and $s(\Delta T_{lmtd}) = 0.043$, the obtained RSS_{Nu} was $\pm2.889\ W/(m^2°C)$. Therefore, the value of RSS_{Nu} is $155.31 \pm 2.889\ W/m^{2°}C$.

The value of h at a speed of 0.4 m/s was found to be 44.86. To determine the standard deviation of Nu the following equation is used

$$RSS_h = \sqrt{\left(s(Nu)\frac{\partial h}{\partial Nu}\right)^2} \quad (17)$$

$$\frac{\partial h}{\partial Nu} = \frac{\partial\left(h.D_h.k^{-1}\right)}{\partial h} = \frac{k}{D_h}$$

Furthermore, the value of D_h is 0.092 m and k at $T_f = 40.24$ is 0.026. So the value of h at a speed of 0.4 m/s is:

$$RSS_h = \sqrt{\left(s(Nu)\frac{\partial h}{\partial Nu}\right)^2} = 0,83$$

Thus, the number h a speed of 0.4 m/s is 44.86 ± 0.83. So, the error h for the baseline at a speed of 0.4 m/s is

$$Error = \frac{RSS_h}{h} \times 100 \quad (18)$$

Table 4
Baseline pressure drop data at a speed of 2.0 m/s.

ΔP (Pa)			
Data to	2.0 m/s	Data to	2.0 m/s
1	0.013	16	0.012
2	0.013	17	0.013
3	0.013	18	0.012
4	0.013	19	0.012
5	0.012	20	0.013
6	0.013	21	0.013
7	0.013	22	0.012
8	0.012	23	0.013
9	0.013	24	0.012
10	0.013	25	0.013
11	0.013	26	0.013
12	0.013	27	0.013
13	0.012	28	0.013
14	0.012	29	0.012
15	0.013	30	0.012

$$Error = \frac{0.83}{44.86} \times 100 = 1.51\%$$

From the test in the baseline case with a speed of 2.0 m/s, the results of the pressure drop are listed in Table 4, which show that the average P can be calculated as follows:

$$\overline{\Delta P} = \frac{\Delta P_1 + \Delta P_2 + \Delta P_3 + \ldots + \Delta P_{30}}{30} = 3.51 \text{ Pa} \quad (19)$$

The average standard deviation of the pressure drop can then be calculated using the equation

$$s = \sqrt{\frac{\sum_{i=1}^{N}(\Delta P_i - \overline{\Delta P})^2}{N(N-1)}} = 8.9 \times 10^{-5} \quad (20)$$

Baseline case for the pressure drop value at a speed of 2.0 m/s is $3.51 \pm 8.9 \times 10^{-5}$ Pa. Then, the error in the form of percentage can be calculated using the following equation:

$$\frac{8.9 \times 10^{-5}}{3.51} \times 100 = 0.71$$

The equal calculation approach changed into used for all data. Therefore, the overall error outputs for the pressure-drop vortex generator with placement variations (in-line and staggered), Re and amount of VG sets (one, two and three) are listed in Table 5.

The average TEF results from the experimental results can be calculated as follows.

$$\overline{TEF} = \frac{TEF_1 + TEF_2 + TEF_3 + \ldots + TEF_{12}}{12} = 1.12 \quad (21)$$

Then, the average standard deviation of the TEF can be calculated with the equation

Table 5
Overall pressure drop (ΔP).

Vortex Generator Variations	Overall Error P (perforated)
1 PRWP *in-line*	2.94%
2 PRWP *in-line*	2.87%
3 PRWP *in-line*	1.98%
1 PRWP *staggered*	2.88%
2 PRWP *staggered*	2.34%
3 PRWP *staggered*	1.36%
1 PCRWP *in-line*	2.72%
2 PCRWP *in-line*	1.80%
3 PCRWP *in-line*	1.80%
1 PCRWP *staggered*	2.43%
2 PCRWP *staggered*	1.91%
3 PCRWP *staggered*	0.97%

Table 6
Overall error *TEF*.

Variasi Vortex Generator	Overall Error TEF (Berlubang)
1 RWP *in-line*	0.47%
2 RWP *in-line*	0.47%
3 RWP *in-line*	0.43%
1 RWP *staggered*	0.47%
2 RWP *staggered*	0.47%
3 RWP *staggered*	0.43%
1 CRWP *in-line*	0.45%
2 CRWP *in-line*	0.45%
3 CRWP *in-line*	0.42%
1 CRWP *staggered*	0.45%
2 CRWP *staggered*	0.45%
3 CRWP *staggered*	0.41%

$$s = \sqrt{\frac{\sum_{i=1}^{N}(TEF_i - \overline{TEF})^2}{N(N-1)}} = 1.07 \quad (22)$$

Therefore, the *TEF* value was 1.12 ± 1.07. Then, the error in the form of percentage can be calculated using the following equation:

$$\frac{1.07}{1.12} \times 100 = 0.94\%$$

The overall error results for the *TEF* vortex generator with placement variations (in-line and staggered), Re and amount of VG sets (one, two and three) are listed in Table 6.

First, find the average *CBR* of the experimental results with the following formula.

$$\overline{CBR} = \frac{CBR_1 + CBR_2 + CBR_3 + \ldots + CBR_{12}}{12} = 2.14 \quad (23)$$

The average standard deviation of the pressure drop *CBR* can then be calculated using the following equation:

$$s = \sqrt{\frac{\sum_{i=1}^{N}(CBR_i - \overline{CBR})^2}{N(N-1)}} = 1.60 \quad (24)$$

The *CBR* value is 2.14 ± 1.60. Then the error in the form of percentage can be calculated using thefollowing equation:

$$\frac{1.60}{2.14} \times 100 = 0.63\%$$

The overall error results for the *CBR* vortex generator with placement variations (in-line and staggered), Re and amount of VG sets (one, two and three) are listed in Table 7.

4. Conclusion

Based on the experimental results for perforated concave rectangular winglet pair vortex generators (PCRWP VGs) used to increase the heat transfer of airflow through heated tubes arranged in-line in the duct, we

Table 7
Overall *error CBR*.

Variasi Vortex Generator	Overall Error CBR (Berlubang)
1 RWP *in-line*	0.32%
2 RWP *in-line*	0.29%
3 RWP *in-line*	0.45%
1 RWP *staggered*	0.32%
2 RWP *staggered*	0.31%
3 RWP *staggered*	0.45%
1 CRWP *in-line*	0.4%
2 CRWP *in-line*	0.42%
3 CRWP *in-line*	0.56%
1 CRWP *staggered*	0.43%
2 CRWP *staggered*	0.42%
3 CRWP *staggered*	0.66%

conclude that using PCRWP VGs affects the convection heat transfer coefficient, pressure drop in achieving hydraulic thermal performance and cost-benefit ratio. In our investigation, the best heat-transfer convection coefficient was 153.5 W/m$^2 \bullet$ K for the three pairs of PCRW VGs, in a staggered manner. The greatest improvement in the pressure drop value (4.58 Pa), occurred for one pair of PCRW VGs arranged in a staggered manner, whereas the hydraulic thermal performance was the best (1.29) in this experiment with the three pairs of PCRW VGs arranged in a staggered manner. Finally, the best CBR (3.56) was recorded for the three pairs of PCRW VGs composed in a staggered manner.

Credit author statement

Oktarina Heriyani: Conceptualization, Methodology, Investigation, Writing – original draft preparation.: Mohammad Djaeni: Supervision – Reviewing and Editing.: Syaiful: Conceptualization, Writing – Reviewing and Editing, Conceptualization.: Aldila Kurnia Putri: Visualisation, Validation.

Declaration of competing interest

The authors declare that they have no known competing financial interests or personal relationships that could have appeared to influence the work reported in this paper.

References

[1] R. Sebayang, AC Akan jadi pengkonsumsi listrik utama di Dunia, CNBC Indonesia (2018).

[2] Z. Qian, Q. Wang, J. Cheng, Analysis of heat and resistance performance of plate fin-and-tube heat exchanger with rectangle-winglet vortex generator, Int. J. Heat Mass Tran. 124 (2018) 1198–1211, https://doi.org/10.1016/j.ijheatmasstransfer.2018.04.037.

[3] D. Mugisidi, O. Heriyani, P.H. Gunawan, D. Apriani, Performance improvement of a forced draught cooling tower using a vortex generator, CFD Lett. 13 (1) (2021) 45–57, https://doi.org/10.37934/cfdl.13.1.4557.

[4] A.J. Modi, N.A. Kalel, M.K. Rathod, Thermal performance augmentation of fin-and-tube heat exchanger using rectangular winglet vortex generators having circular punched holes, Int. J. Heat Mass Tran. 158 (2020) 1–16, https://doi.org/10.1016/j.ijheatmasstransfer.2020.119724.

[5] K.W. Song, T. Tagawa, The optimal arrangement of vortex generators for best heat transfer enhancement in flat-tube-fin heat exchanger, Int. J. Therm. Sci. (2018), https://doi.org/10.1016/j.ijthermalsci.2018.06.011.

[6] C. Yu, H. Zhang, M. Zeng, R. Wang, B. Gao, Numerical study on turbulent heat transfer performance of a new compound parallel flow shell and tube heat exchanger with longitudinal vortex generator, May 2019, Appl. Therm. Eng. 164 (2020), 114449, https://doi.org/10.1016/j.applthermaleng.2019.114449.

[7] M. Samadifar, D. Toghraie, Numerical simulation of heat transfer enhancement in a plate-fin heat exchanger using a new type of vortex generators, September 2017, Appl. Therm. Eng. 133 (2018) 671–681, https://doi.org/10.1016/j.applthermaleng.2018.01.062.

[8] U. Kashyap, K. Das, B.K. Debnath, Effect of surface modification of a rectangular vortex generator on heat transfer rate from a surface to fluid, August 2017, Int. J. Therm. Sci. 127 (2018) 61–78, https://doi.org/10.1016/j.ijthermalsci.2018.01.004.

[9] U. Kashyap, K. Das, B.K. Debnath, Effect of surface modification of a rectangular vortex generator on heat transfer rate from a surface to fluid: an extended study, August, Int. J. Therm. Sci. 134 (2018) 269–281, https://doi.org/10.1016/j.ijthermalsci.2018.08.020.

[10] A.Q. Ibrahim, R.S. Alturaihi, Experimental work for single-phase and two-phase flow in duct banks with vortex generators, Sep, Results in Engineering (2022), 100047, https://doi.org/10.1016/J.RINENG.2022.100497.

[11] K.W. Song, T. Tagawa, Z.H. Chen, Q. Zhang, Heat transfer characteristics of concave and convex curved vortex generators in the channel of plate heat exchanger under laminar flow, November 2018, Int. J. Therm. Sci. 137 (2019) 215–228, https://doi.org/10.1016/j.ijthermalsci.2018.11.002.

[12] K.A. Hammoodi, H.A. Hasan, M.H. Abed, A. Basem, A.M. Al-Tajer, Control of heat transfer in circular channels using oblique triangular ribs, Sep, Results in Engineering 15 (2022), 100471, https://doi.org/10.1016/J.RINENG.2022.100471.

[13] M. Zeeshan, S. Nath, D. Bhanja, A. Das, Numerical investigation for the optimal placements of rectangular vortex generators for improved thermal performance of fin-and-tube heat exchangers, Appl. Therm. Eng. (2018), https://doi.org/10.1016/j.applthermaleng.2018.03.006.

[14] H. Linardos, G. Mavrogenis, D. Margaris, Novel designs of LVGs conformations and introduction of Batch Heated and Channeled Pipe for increasing heat transfer efficiency in pipes, Mar, Results in Engineering 13 (2022), 100357, https://doi.org/10.1016/J.RINENG.2022.100357.

[15] O. Heriyani, M. Djaeni, Syaiful, Thermal-hydraulic performance analysis by means of rectangular winglet vortex generators in a channel: an experimental study, European Journal of Engineering and Technology Research 6 (3) (2021) 150–153, https://doi.org/10.24018/ejers.2021.6.3.2424.

[16] C. Wang, Z. Wang, L. Wang, L. Luo, B. Sundén, Experimental study of fluid flow and heat transfer of jet impingement in cross-flow with a vortex generator pair, Int. J. Heat Mass Tran. 135 (2019) 935–949, https://doi.org/10.1016/j.ijheatmasstransfer.2019.02.024.

[17] Z. Sun, K. Zhang, W. Li, Q. Chen, N. Zheng, Investigations of the turbulent thermal-hydraulic performance in circular heat exchanger tubes with multiple rectangular winglet vortex generators, Mar, Appl. Therm. Eng. 168 (2020), 114838, https://doi.org/10.1016/J.APPLTHERMALENG.2019.114838.

[18] P. Promvonge, S. Skullong, Thermo-hydraulic performance in heat exchanger tube with V-shaped winglet vortex generator, Appl. Therm. Eng. (2020), https://doi.org/10.1016/j.applthermaleng.2019.114424.

[19] S. Skullong, P. Promthaisong, P. Promvonge, C. Thianpong, M. Pimsarn, Thermal performance in solar air heater with perforated-winglet-type vortex generator, June, Sol. Energy 170 (2018) 1101–1117, https://doi.org/10.1016/j.solener.2018.05.093.

[20] Z. Han, Z. Xu, J. Wang, Numerical simulation on heat transfer characteristics of rectangular vortex generators with a hole, Int. J. Heat Mass Tran. 126 (2018) 993–1001, https://doi.org/10.1016/j.ijheatmasstransfer.2018.06.081.

[21] C. Luo, S. Wu, K. Song, L. Hua, L. Wang, Thermo-hydraulic performance optimization of wavy fin heat exchanger by combining delta winglet vortex generators, Appl. Therm. Eng. (2019), https://doi.org/10.1016/j.applthermaleng.2019.114343.

[22] H. Naik, S. Tiwari, Effect of winglet location on performance of fin-tube heat exchangers with inline tube arrangement, Int. J. Heat Mass Tran. 125 (2018) 248–261, https://doi.org/10.1016/j.ijheatmasstransfer.2018.04.071.

[23] M. Zeeshan, S. Nath, D. Bhanja, A. Das, Numerical investigation for the optimal placements of rectangular vortex generators for improved thermal performance of fin-and-tube heat exchangers, May, Appl. Therm. Eng. 136 (2018) 589–601, https://doi.org/10.1016/J.APPLTHERMALENG.2018.03.006.

[24] Y. Effendi, A. Prayogo, Syaiful, M. Djaeni, E. Yohana, Effect of perforated concave delta winglet vortex generators on heat transfer and flow resistance through the heated tubes in the channel, Exp. Heat Tran. 35 (5) (2022) 553–576, https://doi.org/10.1080/08916152.2021.1919245.

[25] S. Whitaker, Forced Convection Heat Transfer Correlations for Flow In Pipes, Past Flat Plates, Single e Cylinders, Single Spheres, and for Flow In Packed Beds and Tube Bundles, Reprillted from, AIChE J. (1972).

[26] M. Awais, A.A. Bhuiyan, Enhancement of thermal and hydraulic performance of compact finned-tube heat exchanger using vortex generators (VGs): a parametric study, Jun, Int. J. Therm. Sci. 140 (2019) 154–166, https://doi.org/10.1016/J.IJTHERMALSCI.2019.02.041.

[27] A. Gupta, A. Roy, S. Gupta, M. Gupta, Numerical investigation towards implementation of punched winglet as vortex generator for performance improvement of a fin-and-tube heat exchanger, Mar, Int. J. Heat Mass Tran. 149 (2020), 119171, https://doi.org/10.1016/J.IJHEATMASSTRANSFER.2019.119171.

[28] M.W. Tian, S. Khorasani, H. Moria, S. Pourhedayat, H.S. Dizaji, Profit and efficiency boost of triangular vortex-generators by novel techniques, Int. J. Heat Mass Tran. 156 (2020), 119842, https://doi.org/10.1016/j.ijheatmasstransfer.2020.119842.

[29] Y.L. He, P. Chu, W.Q. Tao, Y.W. Zhang, T. Xie, Analysis of heat transfer and pressure drop for fin-and-tube heat exchangers with rectangular winglet-type vortex generators, Nov, Appl. Therm. Eng. 61 (2) (2013) 770–783, https://doi.org/10.1016/J.APPLTHERMALENG.2012.02.040.

[30] M. Pranita Hendraswari, M.S. Tony, M.F. Soetanto, Heat Transfer Enhancement inside Rectangular Channel by Means of Vortex Generated by Perforated Concave Rectangular Winglets, 2021, https://doi.org/10.3390/fluids6010043.

[31] A. R. Siwi Syaiful, T.S. Utomo, , Yurianto, R. Wulandari, Numerical analysis of heat and fluid flow characteristics of airflow inside rectangular channel with presence of perforated concave delta winglet vortex generators, International Journal of Heat and Technology 37 (4) (2019) 1059–1070, https://doi.org/10.18280/IJHT.370415.

[32] A. Sinha, H. Chattopadhyay, A.K. Iyengar, G. Biswas, Enhancement of heat transfer in a fin-tube heat exchanger using rectangular winglet type vortex generators, Oct. Int. J. Heat Mass Tran. 101 (2016) 667–681, https://doi.org/10.1016/J.IJHEATMASSTRANSFER.2016.05.032.

[33] H. Ke, et al., Thermal-hydraulic performance and optimization of attack angle of delta winglets in plain and wavy finned-tube heat exchangers, Mar, Appl. Therm. Eng. 150 (2019) 1054–1065, https://doi.org/10.1016/j.applthermaleng.2019.01.083.

[34] A. Arora, P.M.V. Subbarao, R.S. Agarwal, Development of parametric space for the vortex generator location for improving thermal compactness of an existing inline fin and tube heat exchanger, Apr. Appl. Therm. Eng. 98 (2016) 727–742, https://doi.org/10.1016/J.APPLTHERMALENG.2015.12.117.

[35] S. Gururatana, S. Skullong, Heat transfer augmentation in a pipe with 3D printed wavy insert, Oct, Case Stud. Therm. Eng. 21 (2020), 100698, https://doi.org/10.1016/J.CSITE.2020.100698.

[36] A. Sinha, H. Chattopadhyay, A.K. Iyengar, G. Biswas, Enhancement of heat transfer in a fin-tube heat exchanger using rectangular winglet type vortex generators, Oct. Int. J. Heat Mass Tran. 101 (2016) 667–681, https://doi.org/10.1016/J.IJHEATMASSTRANSFER.2016.05.032.

[37] A.J. Modi, M.K. Rathod, Experimental investigation of heat transfer enhancement and pressure drop of fin-and-circular tube heat exchangers with modified rectangular winglet vortex generator, Jun, Int. J. Heat Mass Tran. 189 (2022), 122742, https://doi.org/10.1016/J.IJHEATMASSTRANSFER.2022.122742.

[38] Y. Li, Z. Qian, Q. Wang, Numerical investigation of thermohydraulic performance on wake region in finned tube heat exchanger with section-streamlined tube, May, Case Stud. Therm. Eng. 33 (2022), 101898, https://doi.org/10.1016/J.CSITE.2022.101898.

[39] K. Boukhadia, H. Ameur, D. Sahel, M. Bozit, Effect of the perforation design on the fluid flow and heat transfer characteristics of a plate fin heat exchanger, December 2017, Int. J. Therm. Sci. 126 (2018) 172–180, https://doi.org/10.1016/j.ijthermalsci.2017.12.025. Apr..

[40] C.-H. Huang, L.-W. Liu, Optimal position and perforated radius of punched vortex generators for heat sink, Apr, Case Stud. Therm. Eng. 32 (2022), 101916, https://doi.org/10.1016/J.CSITE.2022.101916.

[41] Y. Menni, et al., Effects of two-equation turbulence models on the convective instability in finned channel heat exchangers, Mar, Case Stud. Therm. Eng. 31 (2022), 101824, https://doi.org/10.1016/J.CSITE.2022.101824.

Oktarina Heriyani - Perforated concave rectangular winglet pair vortex generators enhance the heat transfer of air flowing through heated tubes inside a channel

7   Internet Source   1%

8   www.iieta.org
     Internet Source   1%

9   ejers.org
     Internet Source   1%

10   eprints.undip.ac.id
     Internet Source   1%

11   pastel.archives-ouvertes.fr
     Internet Source   1%

12   www.sysrevpharm.org
     Internet Source   1%

13   Syaiful, Ganesha Rachmandala, Bambang
     Yunianto, MSK Tony Su, M. Ilham Maulana.
     "Heat Transfer Enhancement with Considering
     Pressure Loss Penalty of Airflow through
     Heated Plate Mounted by Perforated Concave
     Rectangular Winglet Vortex Generators", IOP
     Conference Series: Materials Science and
     Engineering, 2019
     Publication   <1%

14   Syaiful, Nakula Kusuma, Muchammad, Retno
     Wulandari, Nazarudin Sinaga, Ahmad
     Siswantara, Myung-Whan Bae. "Numerical
     investigation of heat transfer and pressure
     loss of flow through a heated plate mounted   <1%

by perforated concave rectangular winglet vortex generators in a channel", AIP Publishing, 2020
Publication

15 He, Ya-Ling, Pan Chu, Wen-Quan Tao, Yu-Wen Zhang, and Tao Xie. "Analysis of heat transfer and pressure drop for fin-and-tube heat exchangers with rectangular winglet-type vortex generators", Applied Thermal Engineering, 2012.
Publication

<1 %

16 "Recent Advances in Computational and Experimental Mechanics, Vol II", Springer Science and Business Media LLC, 2022
Publication

<1 %

17 X.L. Zhong, S.C. Fu, K.C. Chan, G. Yang, H.H. Qiu, Christopher Y.H. Chao. "Experimental study on the thermal-hydraulic performance of a fluttering split flag in a channel flow", International Journal of Heat and Mass Transfer, 2022
Publication

<1 %

18 Mallikarjuna Veerabhadrappa Bidari, P. B. Nagaraj, Gururaj Lalagi. "Influence of different types of vortex generators (VGs) to enhance heat transfer performance in heat exchangers: a review", International Journal of Ambient Energy, 2021
Publication

<1 %

19 ebin.pub
Internet Source
<1 %

20 jocpr.com
Internet Source
<1 %

21 Submitted to University of Pretoria
Student Paper
<1 %

22 Tian, L.. "A comparative study on the air-side performance of wavy fin-and-tube heat exchanger with punched delta winglets in staggered and in-line arrangements", International Journal of Thermal Sciences, 200909
Publication
<1 %

23 Zhaoqing Ke, Chung-Lung Chen, Kuojiang Li, Sheng Wang, Chien-Hua Chen. "Vortex dynamics and heat transfer of longitudinal vortex generators in a rectangular channel", International Journal of Heat and Mass Transfer, 2019
Publication
<1 %

24 www.sciencegate.app
Internet Source
<1 %

25 Salviano, Leandro O., Daniel J. Dezan, and Jurandir I. Yanagihara. "Optimization of winglet-type vortex generator positions and angles in plate-fin compact heat exchanger:
<1 %

Response Surface Methodology and Direct Optimization", International Journal of Heat and Mass Transfer, 2015.
Publication

26 krishikosh.egranth.ac.in
Internet Source
<1%

27 Mohd Zeeshan, Sujit Nath, Dipankar Bhanja, Aabir Das. "Numerical investigation for the optimal placements of rectangular vortex generators for improved thermal performance of fin-and-tube heat exchangers", Applied Thermal Engineering, 2018
Publication
<1%

28 Selma Akcay. "Numerical analysis of heat transfer improvement for pulsating flow in a periodic corrugated channel with discrete V-type winglets", International Communications in Heat and Mass Transfer, 2022
Publication
<1%

29 epdf.pub
Internet Source
<1%

30 www.thermalfluidscentral.com
Internet Source
<1%

31 Turo Välikangas, Shobhana Singh, Kim Sørensen, Thomas Condra. "Fin-and-tube heat exchanger enhancement with a combined

herringbone and vortex generator design",
International Journal of Heat and Mass
Transfer, 2018
Publication

32   akademiabaru.com
      Internet Source   <1%

33   ethesis.nitrkl.ac.in
      Internet Source   <1%

34   Syaiful, M. Kurnia Lutfi. "Numerical
      Investigation of Heat Transfer and Fluid Flow
      Characteristics in a Rectangular Channel with
      Presence of Perforated Concave Rectangular
      Winglet Vortex Generators", IntechOpen, 2021   <1%
      Publication

35   dspace.lib.cranfield.ac.uk
      Internet Source   <1%

Exclude quotes   Off   Exclude matches   Off
Exclude bibliography   On